J Biol Inorg Chem
DOI 10.1007/s00775-014-1224-4

ORIGINAL PAPER

Changes in metabolic pathways of *Desulfovibrio alaskensis* G20 cells induced by molybdate excess

Rashmi R. Nair · Célia M. Silveira · Mário S. Diniz · Maria G. Almeida · Jose J. G. Moura · Maria G. Rivas

Received: 28 July 2014 / Accepted: 25 November 2014

Abstract The activity of sulfate-reducing bacteria (SRB) intensifies the problems associated to corrosion of metals and the solution entails significant economic costs. Although molybdate can be used to control the negative effects of these organisms, the mechanisms triggered in the cells exposed to Mo-excess are poorly understood. In this work, the effects of molybdate ions on the growth and morphology of the SRB *Desulfovibrio alaskensis* G20 (*Da*G20) were investigated. In addition, the cellular localization, ion uptake and regulation of protein expression were studied. We found that molybdate concentrations ranging between 50 and 150 μM produce a twofold increase in the doubling time with this effect being more significant at 200 μM molybdate (five times increase in the doubling time). It was also observed that 500 μM molybdate completely inhibits the cellular growth. On the context of protein regulation, we found that several enzymes involved in energy metabolism, cellular division and metal uptake processes were particularly influenced under the conditions tested. An overall description of some of the mechanisms involved in the *Da*G20 adaptation to molybdate-stress conditions is discussed.

Responsible Editors: José Moura and Paul Bernhardt.

R. R. Nair · C. M. Silveira · M. S. Diniz · M. G. Almeida · J. J. G. Moura · M. G. Rivas
REQUIMTE/CQFB,
Departamento de Química,
Faculdade de Ciências e Tecnologia,
Universidade Nova de Lisboa,
2829-516 Caparica, Portugal

M. G. Rivas (✉)
Departamento de Física,
Facultad de Bioquímica y Ciencias Biológicas,
Universidad Nacional del Litoral,
S3000ZAA Santa Fe, Argentina
e-mail: mrivas@fbcb.unl.edu.ar

Keywords Sulfate-reducing bacteria · Hydrogen cycling · Molybdenum · Tungsten · Microbiologically influenced corrosion

Abbreviations

AOR	Aldehyde oxidoreductase
ATP	Adenosine triphosphate
D.	*Desulfovibrio*
*Da*G20	*Desulfovibrio alaskensis* G20
DCPIP	2,6-Dichlorophenol-iodophenol
*Dv*H	*Desulfovibrio vulgaris* Hildenborough
EPS	Extracellular polymeric substance
IEF	Isoelectric focusing
ICP-AES	Inductively coupled plasma atomic emission spectroscopy
MALDI-TOF	Matrix-assisted laser desorption ionization time-of-flight
MIC	Microbiologically influenced corrosion
SEM	Scanning electron microscopy
SRB	Sulfate-reducing bacteria
TCA	Tricarboxylic acid cycle
Tris–acetate/HCl	Tris(hydroxymethyl)aminomethane acetate/hydrochloride
2-DE	Two-dimensional electrophoresis

Introduction

Microbiologically influenced corrosion (MIC) often intensifies the spoilage of pipelines, metal tanks and production equipment leading to significant economic consequences in the gas and oil industries [1–5]. *Desulfovibrio* (*D.*) species are the main microorganisms involved in this process. These bacteria reduce sulfate to hydrogen sulfide; a metabolite highly corrosive to several types of steel and other

Published online: 09 December 2014

alloys [6–8]. Since the industry demands are becoming constantly more severe, the materials need to be stronger and their properties have to be improved to deal with MIC and other corrosion factors.

Diverse strategies have been studied to inhibit the growth of the sulfate-reducing bacteria (SRB). The most common method is the use of chemical biocides which include compounds such as aldehydes (formaldehyde and glutaraldehyde) [9–11], alcohols (bronopol) [12] and surfactants (benzalkonium chloride, cocodiamine) [11, 13]. Due to their broad spectrum of action, these biocides could be toxic to other nontarget species and costly for the environment. The use of less toxic and more specific compounds like nitrate, nitrite or molybdate could overcome this problem [14–16]. Chromate could also be used to control the biogeneration of hydrogen sulfide but due to the toxicity of this compound, molybdate is commonly used to control the SRB activity [17, 18].

Molybdenum is an essential trace element required by biological systems and particularly many important enzymes from *Desulfovibrio* species contain this metal in its active site. To date, several Mo-enzymes were isolated and characterized from *Desulfovibrio* genus including formate dehydrogenases [19–22], nitrate reductases [23], and aldehyde oxidoreductases [24–27] among others. All of them are very important in the *Desulfovibrio* metabolism since they are involved in metabolic pathways that contribute to energy production. The biosynthesis of the enzyme cofactors and the activation of apoenzymes to active forms require transport, activation of molybdate (the most common and stable form of molybdenum) and cofactor incorporation into the apo-molybdenum protein [28, 29]. Despite the relevance of the proteins involved in all these processes, the information about Mo uptake and the control mechanisms developed by SRB to regulate the concentration of this metal in the cell is scarce. In *E. coli*, molybdate is transported to the cell by at least three independent transport systems: a specific transport system encoded by the *mod* gene cluster, the sulfate transport system, and a nonspecific transport system [30]. The specific transport system encoded by the *modABC* operon is induced only under molybdate starvation and is repressed in presence of molybdate by the ModE–molybdate complex [31]. Nevertheless, under high molybdenum concentration, cells can incorporate the metal by the other two machineries [30]. An analysis of the *D. alaskensis* G20 (*Da*G20) genome shows that *mod* genes are also present in this organism suggesting that cells incorporate Mo by similar transport systems [32, 33]. By analogy with the metal transport systems described for *E.coli*, it can be supposed that the inhibition of this SRB by molybdenum-excess is started by the nonspecific uptake of molybdate [33]. Once the oxoanion is in the cell, it is known that the ATP (adenosine triphosphate) sulfurylase enzyme can bind molybdate which avoids sulfate activation and consequently inhibits the respiratory chain [34].

The present work is aimed to evaluate the effects of molybdenum-excess on *Da*G20 cells. The influence of molybdate-stress conditions on the cell growth, ion uptake, cellular morphology and regulation of protein expression was studied and discussed.

Materials and methods

Cell culture conditions

To study the influence of molybdenum-excess on the *Da*G20 growth, cells were cultured at 37 °C under anaerobic conditions in medium C from Postgate [35] supplemented or not with different $Na_2MoO_4{\cdot}2H_20$ concentrations (50, 100, 150, 200 and 500 µM). To remove the oxygen, the medium was boiled, dispensed serum bottles with rubber stoppers, purged with pure argon for 30 min and finally autoclaved at 121 °C at 20 psi for 20 min. Each culture was performed in triplicate and the medium (90 mL) was inoculated with 10 mL of a *Da*G20 culture grown till exponential phase. The growth time courses were evaluated by measuring the optical density at 600 nm in a Shimadzu UV-160 spectrophotometer. The condition showing 70 % of growth inhibition (100 µM $Na_2MoO_4{\cdot}2H_20$) was used in the studies described below.

Protein sample preparation for two-dimensional electrophoresis (2-DE), aldehyde oxidoreductase (AOR) activity tests and metal uptake evaluation.

D. alaskensis G20 cells were grown in medium C from Postgate [35] under normal (without molybdate supplementation) and stress conditions (medium supplemented with 100 µM $Na_2MoO_4{\cdot}2H_20$) in 2 L flasks adapted to anaerobic growth at 37 °C. Late log phase cells (20 h growth) were harvested by centrifuging (Beckman Coulter Avanti J-26 XPI) for 30 min at 7,000×*g*. The cells were extensively washed by resuspension in 5 mM Tris–acetate buffer (pH 8.0) supplemented with protease inhibitor (1 tablet per 50 mL cell suspension, complete EDTA-free, Roche) and centrifugation at 7,000×*g* for 30 min. The pellet was resuspended (1 g cells per 3 mL buffer) in the buffer/protease inhibitor solution described above, also supplemented with DNAse and RNAse (5 µg/mL each). The cell suspension was frozen and thawed thrice, disrupted using a French press cell at 15,000 psi and centrifuged again for 30 min at 7,000×*g*. The supernatant was then ultracentrifuged (Beckman Coulter Optima™ LE-80K, 70Ti Rotor) for 45 min at 45,000 × rpm to separate the soluble and membrane fractions. All these steps were performed at 4 °C. These

fractions were used for further 2-DE studies, AOR activity tests and metal uptake evaluation.

Two-dimensional gel electrophoresis

A known amount of protein (see below) was diluted in rehydration buffer (7 M urea, 2 M thiourea, 2 % CHAPS (w/v), 0.5 % IPG buffer pH 3–10 (GE-Healthcare), 0.28 % dithiothreitol), loaded in 18 cm Immobiline Drystrip gels pH 3–10 NL (GE-Healthcare) prehydrated overnight with 340 µl of rehydrating buffer and focused in an isoelectric focusing (IEF) system (Ettan IPGphor 3, GE-Healthcare). During the first dimension, the voltage was increased according to the following program: 300 V (900 V/h), 1,000 V (gradient 3,900 V/h), 10,000 V (gradient 16,500 V/h), and 10,000 V (30,000 V/h). Strips were then equilibrated at room temperature in two steps for 10 min each. First, they were incubated in a solution containing 1 % (wt/vol) dithiothreitol to reduce the proteins and sulfhydryl groups and then were derivatized using 2.5 % (wt/vol) iodoacetamide. Both reductant and derivatizing solutions were prepared in 50 mM Tris–HCl pH 8.8, 6 M urea, 30 % (vol/vol) glycerol, 2 % (wt/vol) sodium dodecyl sulfate and bromophenol blue. For the second dimension, proteins were separated on 12.5 % polyacrylamide gels containing 0.2 % (wt/vol) sodium dodecyl sulfate in Ettan DALTsix system (GE-Healthcare) and stained. In the case of proteomic profile analysis, 60 µg of protein was analyzed and gels were silver stained according to the protocol described by Heukeshoven and Dernick [36]. Gels used for protein identification were loaded with approximately 450 µg of total protein and stained using colloidal Coomassie staining [37]. Total protein concentration of the soluble extracts was measured by Bradford protein assay (BIO-RAD Protein Assay kit). In both cases, gels were scanned and digitized using Imagescanner II and ImageMaster2D software from GE-Healthcare. Spot densities on three gel images from three independently grown cultures were compared between the control and the experimental samples. The intensity level of the spots was determined by the relative spot volume of each protein compared to the normalized volume of the spots. A twofold change in relative spot volume was used to determine if proteins were significantly differentially expressed under the two conditions. Spots showing a higher intensity and those observed only in one experimental condition were selected for protein identification by MALDI-TOF mass spectrometry.

Protein identification by MALDI-TOF mass spectrometry

Protein spots of interest were manually excised (from Coomassie stained gels), the gel pieces were placed in microfuge tubes, washed, dried and in-gel digested by trypsin as described in Ref. [38]. The trypsin digested samples were analyzed by Matrix-assisted laser desorption ionization time-of-flight mass spectrometry (Ultraflex II MALDI-TOF TOF Bruker–Daltonics equipped with a LIFT cell and N2 laser). Peak list and spectral processing were done in FlexAnalysis 3.0 (Bruker Daltonics). Protein identification was carried out using MASCOT (Matrix Science, London, UK) and the identified proteins were then analyzed using the IMG system program (http://img.jgi.doe.gov). Their probable role in the *Desulfovibrio* metabolic pathways was deducted using the KEGG (Kyoto Encyclopedia of Genes and Genomes) pathway maps.

Aldehyde oxidoreductase activity

Soluble protein fractions of stressed (100 µM molybdate) and nonstressed *Da*G20 cells were analyzed for AOR activity. Assays were performed aerobically at 37 °C in a quartz cell equipped with a magnetic stirrer according to the procedure described by Thapper et al. [24]. The incubation mixture comprised 35 µM 2,6-dichlorophenol-iodophenol (DCPIP), 50 mM Tris–HCl buffer pH 7.6 and 1.4 µg protein sample. The reaction was initiated by addition of the substrate (120 µM benzaldehyde) and the activity was determined spectrophotometrically at 600 nm. Controls were performed in the same conditions described but without substrate addition.

The AOR activity assay described before was adapted to perform a gel activity test of the soluble protein fractions of stressed (100 µM molybdate) and nonstressed *Da*G20 cells. Samples were prepared in sample buffer [0.5 M Tris–HCl (pH 6.8), 10 % (vol/vol) glycerol, 0.002 % (wt/vol) bromophenol blue] and loaded on native 7.5 % polyacrylamide gels. The electrophoresis was carried out at 150 V and gels were then incubated with 350 µM DCPIP at 37 °C for 30 min till the gel became completely blue. The reagent was removed and replaced by a substrate solution (850 µM benzaldehyde). The gel was incubated with shaking till a colorless band was observed which indicates AOR activity.

Scanning electron microscopy (SEM) analysis

To investigate any morphological changes or formation of molybdate residues at the periphery of the molybdate-stressed cells, high-resolution electron microscopy was used. *Da*G20 cells cultured in medium C from Postgate [35] supplemented with 100 µM molybdate were collected by centrifugation at late log phase and washed with 0.1 M sodium phosphate buffer (pH 7.2). The cells were fixed by incubating the cell pellet in a solution containing 2.5 % glutaraldehyde in 0.1 M sodium phosphate buffer (pH 7.2)

overnight at room temperature. They were then washed with 0.1 M sodium phosphate buffer (pH 7.2), postfixed with 4 % OsO_4 and dehydrated in an ascending gradient of ethanol (30–100 %). The samples were finally incubated in hexamethyl disilazane at 35 °C for 5 min, mounted on silicon chips, air dried and examined under the scanning electron microscope (Zeiss Auriga).

Molybdenum and protein content in soluble and membrane cell fraction

To evaluate molybdenum uptake/accumulation in *Da*G20 cells, molybdenum was determined in soluble and membrane fractions and related to total protein concentration. The experiments were carried out in samples obtained from two independent cultures and three dilutions were performed from each sample. Molybdenum concentration was determined by ICP-AES in a Jobin–Yvon (Ultima) instrument. Standard metal solutions ranging from 0.02 to 1.00 ppm were prepared from 23 ICP Multi Element Standard in 5 % HNO3 and 0.2 % HF (Reagecon).

Protein concentration was also determined on both stressed and normal samples using the Bradford protein assay (BIO-RAD Protein Assay kit). Error bars in Fig. 6 were calculated considering molybdenum and protein determinations as indirect measurements, i.e., by propagation of error.

Results and discussion

Effects of molybdate on *Da*G20 growth

To determine the tolerance levels of *Da*G20 to molybdate, growth studies were carried out in medium C from Postgate [35] supplemented with different molybdate concentrations (50–500 μM). The concentration of molybdenum in the culture medium not supplemented was found to be less than 10 nM as determined by ICP-AES.

As depicted in Fig. 1 and Table 1, the presence of molybdate in the culture medium decreases the growth rate and consequently increases the doubling time of the cultures. Molybdate concentrations ranging between 50 and 150 μM produced a twofold increase in the doubling time and a decrease in the growth rate. This effect becomes more dominant at molybdate concentrations higher than 150 μM showing a five times increase in the doubling time at 200 μM molybdate and complete inhibition of the cellular growth at 500 μM molybdate. Taking into account these results, 100 μM molybdate was considered as the sublethal level of Mo stress and all further experiments were carried out under this condition.

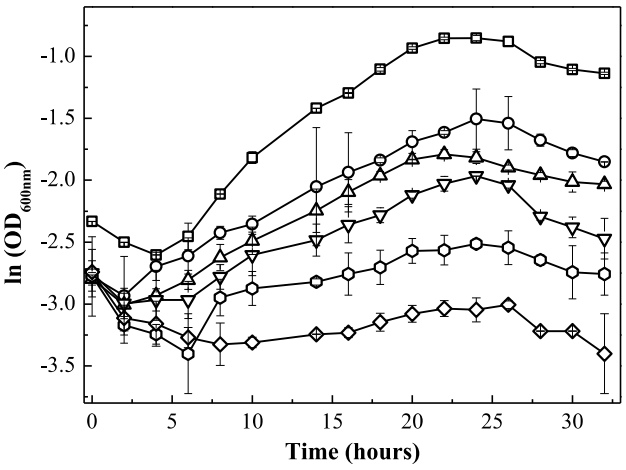

Fig. 1 Growth curves of *Da*G20 cultured in medium C from Postgate [31] supplemented or not with different concentrations of sodium molybdate: 0 μM (*square*), 50 μM (*circle*), 100 μM (*triangle*), 150 μM (*inverted triangle*), 200 μM (*hexagon*) and 500 μM (*rhombus*). Each growth curve was performed in triplicate. The *error bars* added correspond to the error with a confidence interval of 80 % for student's *t* distribution

Differential protein expression in *Da*G20 cells grown under molybdate excess

Two-dimensional gel electrophoresis was carried out to determine the proteomic changes in *Da*G20 cells grown in medium containing 100 μM molybdate (Fig. 2). The protein profile of the soluble fraction from molybdate-stressed cells was compared with the one obtained from nonstressed (normal) cells. The results show that under molybdate excess, a significant downregulation of proteins occurs. A total of 790 ± 60 and 490 ± 40 spots were detected in the soluble fraction of nonstressed and stressed cells (Fig. 2a, b). Besides this clear difference, 49 ± 4 more spots decreased their intensity in the molybdate-stressed cells, whereas 52 ± 3 protein spots were more intense in this condition (20 ± 2 were upregulated and 32 ± 2 were only present in Mo stressed gels).

Spots showing differential intensities (increasing or decreasing) and those detectable only in nonstressed cells were excised for further identification. Both the molecular weight and isoelectric point of each identified protein were calculated according to the primary amino acid sequence of the identified protein and correlated with the experimental results.

As shown in Tables 2, 3 and 4, the main effect caused by molybdenum stress was the downregulation and/or repression of several proteins mainly involved in energy metabolism, cell division and metal homeostasis. The involvement of the relevant proteins on the different metabolic pathways

Table 1 Dependence of growth rate and doubling time of *Da*G20 cells on molybdate concentration

Molybdate concentration (μM)	0	50	100	150	200	500
Growth rate (h^{-1})	0.135 (3)	0.061 (1)	0.068 (1)	0.060 (3)	0.028 (3)	0.030 (3)
Doubling time (h)	5.2 (1)	11.4 (2)	10.3 (1)	11.6 (1)	25.1 (3)	23.3 (2)

The numbers in the parentheses are the standard deviation values for the last significant digit of the estimated parameters

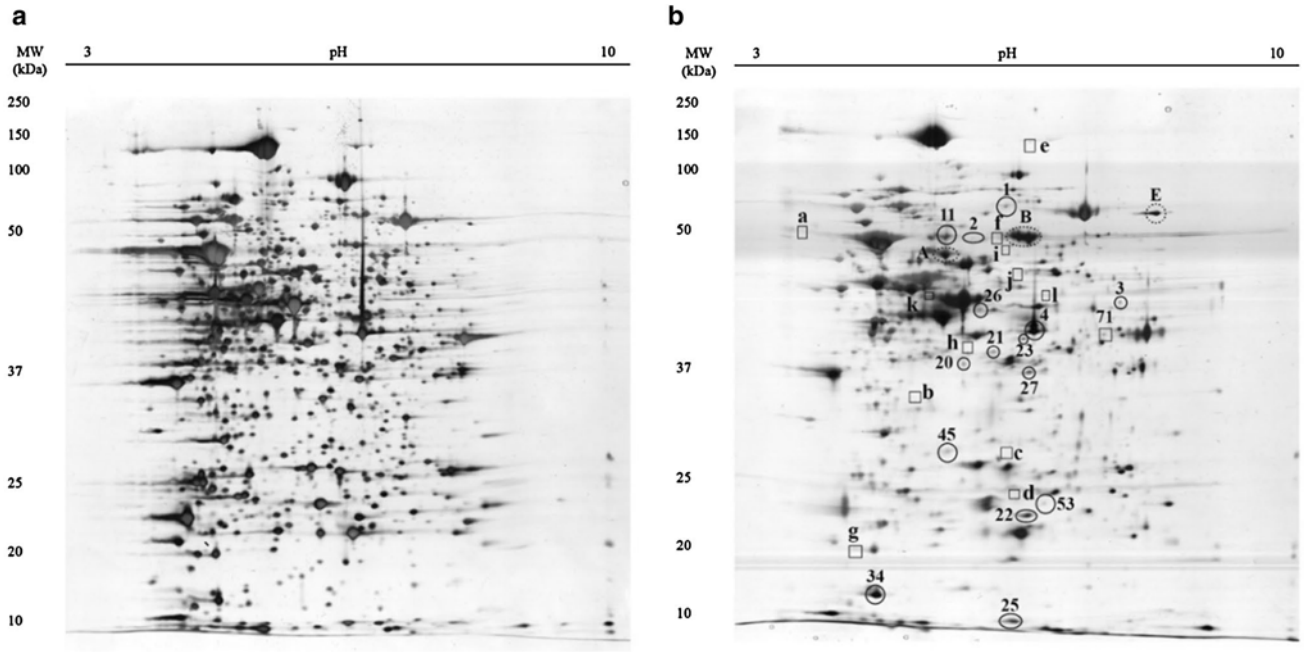

Fig. 2 Overview of the 2-DE of the soluble fractions from *Da*G20 cells grown in medium (**a**) without molybdate (**b**) supplemented with 100 μM molybdate. *Squares* proteins found only in nonstressed condition; *dashed circles* overexpressed proteins; *complete circles* underexpressed proteins. Each two-dimensional gel electrophoresis is representative of three independent experiments. Gels were loaded with 60 μg of protein and silver stained. Differential image analysis was performed using ImageMaster2D software from GE-Healthcare

and cellular processes are discussed in the following sections.

Proteins involved in energy metabolism and energy conservation

Proteomic analysis allows us to identify at least five proteins upregulated under of molybdate-stress conditions involved in energy metabolism/conservation (Table 2): the [NiFe] hydrogenase-1 (Dde_2137), the MopB/QrcB (Dde_2933), the CoB–CoM heterodisulfide reductase (Hdr/Qmo, Dde_1208), the W-aldehyde oxidoreductase (AOR, Dde_2460) and the CO dehydrogenase (CODH, Dde_3028).

The upregulation of both [NiFe] hydrogenase-1 (Dde_2137) and MopB (Dde_2933) protein could be associated to the requirement of energy (ATP) and to solve the problems related with the accumulation of reducing equivalents. Under the conditions tested in this work, ATP sulfurylase uses molybdate (instead of sulfate) and ATP to produce an unstable molecule equivalent to adenosine 5′-phosphosulfate (APS) that cannot be used as electron acceptor [17, 34]. On the other hand, the multiple-step oxidation of lactate produces electrons and protons [39]. Under normal growth conditions the electrons are used to reduce sulfate, however, under molybdate-stress conditions it could be postulated that these electrons and protons are driven to the hydrogen cycle [40, 41] to produce H_2 (reaction catalyzed by hydrogenases). Then, the H_2 produced can diffuse to the periplasmic side of the membrane where it is re-oxidized to protons by periplasmic hydrogenases (like [NiFe] hydrogenase-1, Dde_2137, identified in the present work). Translocation of protons to the cytoplasm and the consequent ATP synthesis could help to balance the energy lost. Moreover, the electrons coming from hydrogen oxidation could be then transferred to the *c*-type cytochrome network for delivery through the cytoplasmic membrane via membrane-bound electron carriers for proton reduction

Table 2 Proteins induced twofold or more in protein extracts from cells grown in the presence of 100 μM molybdate

Cellular role	Subrole	Name	Spot id	Locus tag	PI	Mr (kDa)	Mascot score	% Sequence cover	Change[a]
Energy metabolism	Glycolysis/gluconeogenesis	Aldehyde: ferredoxin oxidoreductase tungsten containing	A	Dde_2460	5.4	160	176	41	20.4
	TCA cycle	CoB–CoM heterodisulfide reductase, subunit B (Hdr/Qmo)[b]		Dde_1208	5.25	31	128	61	3.24
	Hydrogen metabolism	[NiFe] Hydrogenase small subunit[b]		Dde_2137	5.54	34	64	35	3.24
	Electron transfer reactions	Molybdopterin oxidoreductase, molybdopterin-binding subunit (Mop/Qrc)	E	Dde_2933	7.22	72	103	20	9.11
Cell generation and energy conservation	Assimilation of carbon	CO dehydrogenase catalytic subunit	B	Dde_3028	5.91	65	108	27	6.66
Cellular processes	Cell division	ParA/MinD ATPase-like protein[b]	31	Dde_3202	5.40	42	123	42	3.24
Transport proteins	RND family efflux transporter	HIyD	C	Dde_0402	7.9	42.6	176	51	3.06

[a] Relative intensity ratio over the nonstressed cells

[b] Proteins found in the insoluble fraction probably due to the putative association to complex systems in the membrane fraction

(or sulfate under normal conditions). Many such membrane proteins and transmembrane complexes have been proposed as possible electron transfer channels for transferring electrons across the cytoplasmic membrane. Transposon mutagenesis studies had earlier identified a *Da*G20 mutant with an insertion in the gene coding for the component B of the MopABCD protein complex (locus tag Dde_2933 in the present study) which was unable to grow using H_2 or formate as electron donor [42]. In addition, the isolation and characterization of the homologous *Dv*H protein complex [named as quinone reductase complex (Qrc) ABCD] [43] demonstrated that this complex is efficiently reduced by periplasmic hydrogenases and formate dehydrogenases through the type I cytochrome c_3 and interacts with quinones. Evidences from both studies support the presence of a metabolic pathway in which periplasmic hydrogenases (like [NiFe] hydrogenase-1, Dde_2137, identified in the present work) and Mop/Qrc complex are highly relevant. The results found in the present work support the putative interaction between hydrogenases ([NiFe] hydrogenase-1, Dde_2137) and the Mop/Qrc complex as well as the role of these proteins in the cell growth under molybdate-stress conditions.

Our studies had also shown an increase in the expression levels of an enzyme annotated as CoB–CoM heterodisulfide reductase (Hdr) under molybdate excess (Dde_1208, Table 2). Since this enzyme is homologous to the Qmo (DVU0848-0850) identified in the closely related *Dv*H organism, it could be postulated a function linking the electron transport from hydrogen oxidation in the periplasm (Fig. 3) [44, 45].

Desulfovibrio spp. growing on lactate- and sulfate-containing medium produces metabolites such as H_2, formate and CO. The production and consumption of CO was observed in *Dv*H which encodes a cytoplasmic CO dehydrogenase that together with a CO-dependent hydrogenase converts CO to CO_2 and H_2 [41]. In the present work, the upregulation of the CO dehydrogenase (CODH, Dde_3028, Table 2) could be also related to the increasing reducing equivalent flow through hydrogen cycling. Again, molecular hydrogen diffuses across the membrane to be oxidized to protons by hydrogenases. These protons will form a proton gradient used for additional ATP synthesis (Fig. 3).

Another interesting fact observed was the overexpression of a W-aldehyde oxidoreductase (AOR, Dde_2460, Table 2) in a rich Mo-containing medium. Since Mo and

Table 3 Proteins under expressed in extracts from *Da*G20 cells grown in medium supplemented with 100 μM molybdate

Cellular role	Subrole	Name	Spot id	Locus tag	PI	Mr (kDa)	Mascot score	% Sequence cover	Change[a]
Energy metabolism		Alcohol dehydrogenase	21	Dde_0050	5.59	42	97	34	−3.06
	TCA cycle	Succinate dehydrogenase subunit C	b	Dde_1208	5.25	31	110	53	−6.59
		PBS lyase HEAT like repeat	a	Dde_1572	4.53	70	72	20	−4.02
Aminoacid, purines, pyrimidines, nucleosides and nucleotides biosynthesis	Valine, Leucine, Isoleucine biosynthesis	Acetolactate synthase large subunit	i	Dde_2168	5.78	60	195	53	−2.90
	Salvage of nucleosides and nucleotides	Adenine deaminase	11	Dde_0136	5.33	60	124	46	−2.00
	Cysteine and methionine metabolism	Cysteine synthase A	20	Dde_3080	5.54	33	142	50	−2.00
Protein fate	Aminoacylase activity, hydrolase activity, metallopeptidase activity	M20/M25/M40 family peptidase	h	Dde_1186	5.46	39	174	62	−5.53
Transport and binding proteins	Molybdate transport system	Molybdenum ABC transporter, periplasmic molybdate binding protein	53	Dde_0155	6.59	26	94	42	−6.19
		Molybdenum ABC transporter, periplasmic molybdate binding protein (Mod A)	45	Dde_3518	6.59	27	73	39	−2.07
	Phosphonate transport system	Phosphonate binding periplasmic protein (Phn D)	27	Dde_3730	6.26	37	126	38	−2.14

[a] Relative intensity ratio over the nonstressed cells

Table 4 Proteins only detected under normal conditions

Cellular role	Subrole	Name	Spot id	Locus tag	PI	Mr (kDa)	Mascot score	% Sequence cover
Energy metabolism	TCA cycle	Pyruvate carboxylase	e	Dde_2081	5.89	137	139	27
	Histidine metabolism	Imidazole glycerol phosphate synthase subunit HisH	d	Dde_0332	5.78	22	78	43
	Methanogenesis	Tungsten formylmethanofuran dehydrogenase family protein/molybdopterin-binding protein	2	Dde_0685	5.57	60	102	23
Cell cycle	DNA replication and packaging during cell division	HMGL like domain containing protein	f	Dde_0520	5.64	68	158	41
Stress response	Defense against alkyl and lipid hydroperoxides	Thiol peroxidase (atypical 2-cys peroxiredoxin)	g	Dde_2313	4.89	18	226	78
Amino acid, purines, pyrimidines, nucleosides and nucleotides biosynthesis	Valine, Leucine, Isoleucine biosynthesis	2-Isopropylmalate synthase	j	Dde_3218	5.88	54	136	42
	Lysine biosynthesis. Secondary metabolites biosynthesis	Dihydrodipicolinate reductase	c	Dde_2092	5.70	27	98	47
	Pyrimidine nucleotides biosynthesis	Dihydroorotase	l	Dde_2965	5.81	45	93	38

W share several chemical characteristics, the cell needs to carefully control the correct metal insertion in enzymes. However, in some cases the control mechanisms can be evaded and W-replacement by Mo, or viceversa, yields less efficient and even inactive enzymes [46–49]. To further investigate this phenomenon, the correlation between protein production and enzyme activity was evaluated (see AOR activity section).

As observed in this and other works, stress responses often result in growth inhibition which could be associated to decrease in energy production [50]. In the present study, at least three important enzymes which play a crucial role in energy generation showed a downregulation or repression under Mo stress (Tables 3 and 4). They are involved in energy production (alcohol dehydrogenase, Dde_0050), in pyruvate catabolism pathway as an intermediate in oxaloacetate and pyruvate (pyruvate carboxylase, Dde_2081) and probably in the use of alternative substrates as electron donors (tungsten formylmethanofuran dehydrogenase family protein, Dde_0685). The downregulation of these enzymes is in agreement with low cell growth under high levels of molybdate found during growth studies. Genes involved in energy metabolism generally have lower expression during stress conditions like carbon or nitrate limitations, heat shock or oxidative stress [51–54].

Metal homeostasis

As shown in Table 3, periplasmic components from ABC type of transporters were downregulated under stress with molybdate. In line with the fact that the *modABC* operon is translated only under molybdate starvation and repressed under molybdate excess [20, 31], the expression of two periplasmic proteins from the ModABC systems (ModA isoenzymes loci tag Dde_0155 and Dde_3518, respectively, Table 3) involved in molybdate transport was decreased. In addition, the expression of the periplasmic tungstate binding protein (TupA locus tag Dde_0234) is shown to be slightly downregulated (data not shown). It is known that the expression of Mod proteins is regulated by a protein encoded upstream the *modABC* operon, known as ModE [31]. One of the questions that remain to be answered is whether there exists a ModE equivalent for TupABC systems. A recent work suggests that in *Dv*H this role is played by a novel tungstate responsive regulator (TunR, locus tag DVU0179) which controls the homeostasis of both molybdate and tungstate in the cell [55].

Amino acid and nucleotides metabolism

Some of the proteins involved in nucleic acid and amino acid biosynthesis like acetolactate synthase (Dde_2168),

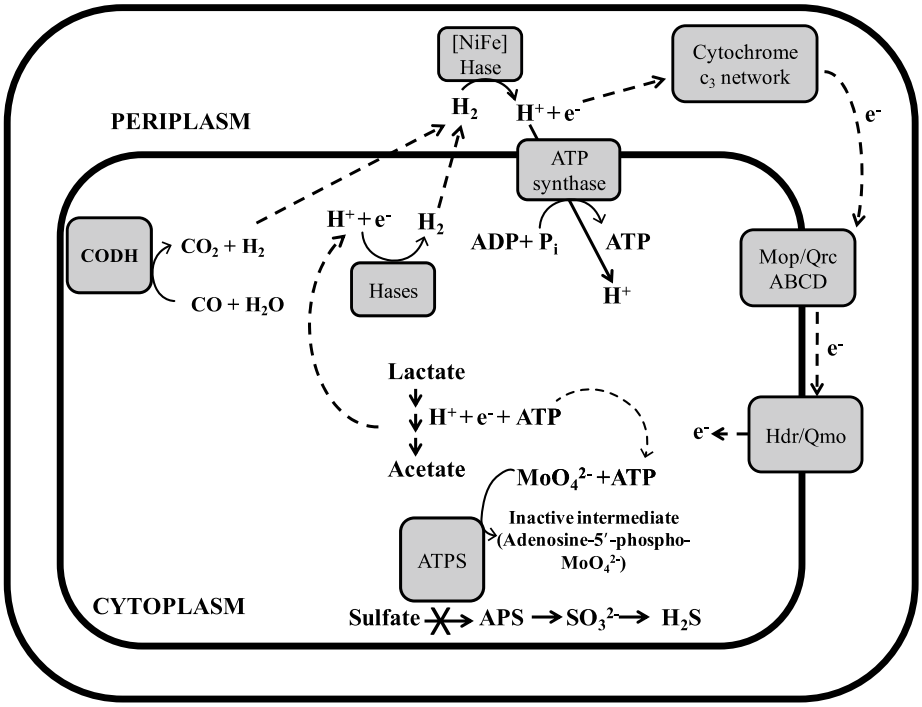

Fig. 3 Proposed electrons and protons pathway in *Da*G20 cells grown under molybdate-stress conditions. *ATPS* ATP sulfurylase, *CODH* carbon monoxide dehydrogenase, *Hase(s)* hydrogenase(s), *Hdr/Qmo* heterodisulfide reductase/quinone-interacting membrane-bound oxidoreductase, *Mop/Qrc* molybdopterin oxidoreductase

adenine deaminase (Dde_0136) and cysteine synthase A (Dde_3080) were found to be downregulated in cells stressed with molybdate (Table 3). Studies have shown the formation of molybdenum sulfide complexes in the cells grown in excess of molybdenum [17]. Since cysteine synthase A is involved in cysteine biosynthesis which requires sulfide as a major precursor, the downregulation of this protein could be associated with the unavailability of this compound.

Similarly, the combined repression of proteins like dihydrodipicolinate reductase (lysine biosynthesis, locus tag Dde_2092) and 2-isopropylmalate synthase (valine, leucine and isoleucine biosynthesis, locus tag Dde_3218) is in line with the general decrease of protein expression observed by two-dimensional gel analysis (Fig. 2).

Dihydroorotase (Dde_2965), a zinc metalloenzyme that catalyzes the reversible interconversion of carbamoyl aspartate and dihydroorotate during pyrimidine nucleotides biosynthesis, was found to be repressed in this study. This was also observed in *Dv*H under oxidative stress conditions. The study suggested the possibility of metal catalyzed oxidation reactions affecting enzymes that require a divalent metal ion for activity [56].

Other cellular processes

Cells cultured under molybdate excess showed upregulation of MinD ATPase (Dde_3202, Table 2). This result is in line with other works in which the overproduction of this protein is associated with the inhibition of cellular division [57, 58], thereby causing low cell growth as observed in Fig. 1. In agreement with this result, decrease of the production of a protein involved in DNA replication and packaging during cell division (HMGL like domain containing protein, Dde_0520, Table 4) was observed.

Under molybdate excess, the upregulation of the secretion protein HIyD (Dde_0402, Table 2) which belongs to the RND (resistance–nodulation–cell division) family efflux of transporters was observed. Efflux systems in bacteria have been found to have a strong impact on antimicrobial resistance mechanisms [59] catalyzing export of heavy metals, multiple drugs and lipooligosaccharides (in plants). Therefore, the expression pattern observed in *Da*G20 is compatible with resistance mechanisms against molybdate excess.

AOR activity

The W-containing AOR showed higher expression levels under molybdate-stress conditions as compared to non-stressed conditions (Table 2, Dde_2460). To evaluate and correlate the upregulation of this W-containing enzyme, AOR activity was measured in the soluble fraction of cells grown under both molybdate-stress and normal conditions. Unlike the proteomic studies, very low activity was detected in the molybdate-stressed cells (Fig. 4a). This result was further confirmed by qualitative studies that detect AOR activity in native polyacrylamide gels (Fig. 4b). The fact that an increase of the AOR production is not compatible with a decrease in enzymatic activity could be due

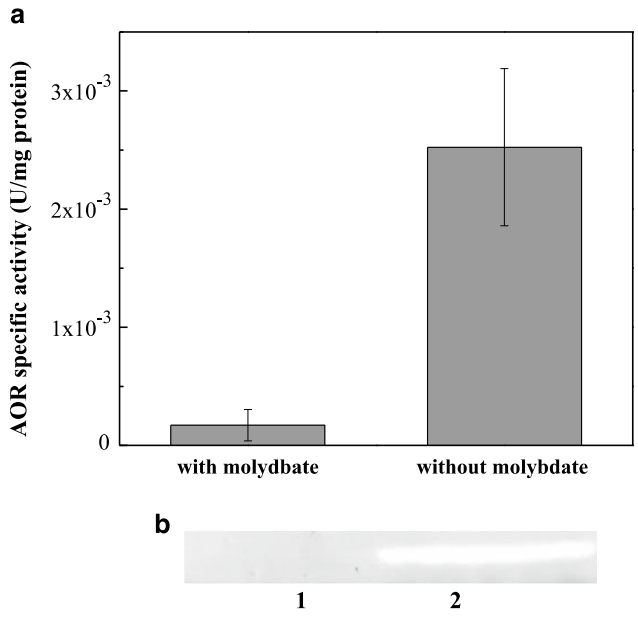

Fig. 4 **a** AOR-specific activity (μmoles/min/mg protein) of the soluble fraction of *Da*G20 cells grown in Postgate C medium without molybdate and with 100 μM molybdate, respectively. **b** In-gel AOR activity of soluble fractions of *Da*G20 cells grown in Postgate C medium [31] *1* without molybdate and *2* with 100 μM molybdate

to a nonspecific incorporation of Mo instead of W in the active site of the enzyme. Although this hypothesis needs to be further explored, this is not the first case were the substitution of W by Mo (or viceversa) yields inactive AOR enzyme [48].

Evaluation of the molybdenum uptake and morphology of cells grown under molybdate stress conditions

The use of electron microscopy to study morphological and surface details on bacterial cells due to environmental stress has been reported by several authors [17, 60, 61]. Biswas et al. [17] detected the presence of electron dense material in the periplasm of *D. desulfuricans* cells which revealed formation of molybdenite (molybdenum sulfide) deposits on cells grown in medium supplemented with Mo. Similarly, formation of EPS (extracellular polymeric substances) around the cells indicates metal sorption as these compounds has a tendency to bind metals [62, 63]. In the present work, Scanning Electron Microscopy (SEM) was used to study the morphological changes on cells culture in medium supplemented with molybdate. As shown in Fig. 5, neither changes in the morphology nor electron dense material deposits or EPS were observed on molybdate-treated cells.

In the light of these results, the uptake and localization of molybdenum in the cell were studied. Membrane and soluble protein fractions were obtained as described in Sect. "Materials and Methods" and the ratio Mo mass/protein mass was calculated for each fraction. The results show that molybdenum atoms are incorporated by the cells and accumulated in both soluble and membrane fractions (Fig. 6). Molybdenum was also quantified in the molybdate-supplemented Postgate C medium after cell culture showing a concentration of 68 ± 12 μM showing that at around 30 % of the molybdenum present in the culture medium is incorporated by the cells.

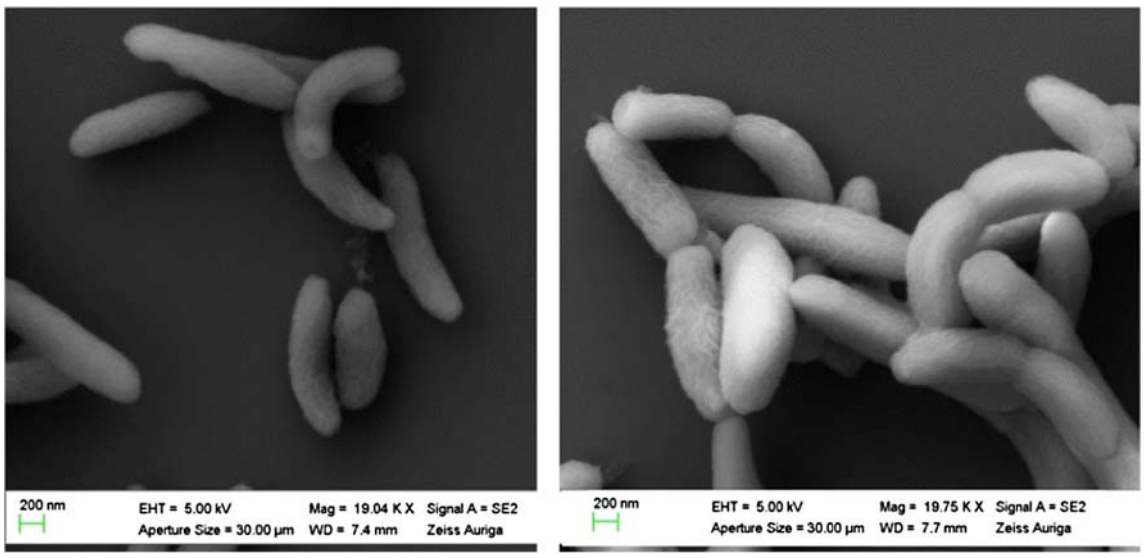

Fig. 5 SEM micrographs of *Da*G20 cells grown in medium C from Postgate [31] without molybdate (*left*) and with 100 μM molybdate (*right*)

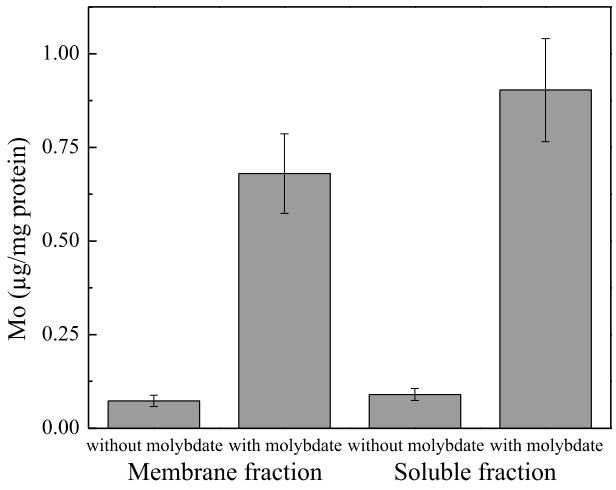

Fig. 6 Molybdenum concentration in membrane and soluble fractions of *Da*G20 cells grown under Mo stress determined by ICP-AES. *Error bars* were determined by propagation of error, it means considering molybdenum and protein determinations as indirect measurements

Conclusions

SRB are the main organisms contributing to corrosion processes, a problem with severe economic consequences in both oil and gas industries [1–5]. Although the control of these bacteria can be successfully achieved by the addition of molybdate to the culture medium [18], the molecular mechanisms triggered in the SRB to survive these adverse conditions are poorly understood. In this work, we study the effects of increase of molybdate concentration on the *Da*G20 growth, the metabolic pathways affected and the cellular uptake of molybdenum. We observed that as the concentration of the metal ion increases, the *Da*G20 growth rate decreases showing clearly the negative effect of the oxoanion on the growth of this SRB. The effect of molybdate on other *Desulfovibrio* species is similar but the concentration impairing the cellular division varies [16]. Though morphological changes are not visible at 100 µM molybdate, the proteome of *Da*G20 cells under the stress conditions tested is largely affected. Regarding the proteins involved in energy production processes, it seems that an increase of the flow of the reducing equivalents and molecular hydrogen through hydrogen cycling is activated to solve the problem associated with the ATP sulfurylase inhibition by molybdate ions. In addition, our results also showed that despite the mechanisms developed by the cell to avoid massive incorporation of molybdate, a large amount of it still entered the cell (approximately, 30 % of the molybdate added to the culture medium was incorporated). The cellular localization of molybdenum after uptake is not completely clear.

Although extensive studies need to be performed on this subject, the results presented contribute to the knowledge about the mechanisms induced in the SRB to survive adverse environment conditions and this could help further to design more specific environment friendly strategies to control biocorrosion processes.

Acknowledgments This work was supported by Fundação para a Ciência e Tecnologia (EXPL/BBB-BEP/0274/2012). We thank Carla Rodrigues (Chemistry Department, FCT, UNL) for inductively coupled plasma atomic emission spectroscopy (ICP-AES) analysis. RRN and CMS thank FCT for Post-doctoral grants (References SRFH/BPD/63061/2009 and SRFH/BPD/79566/2011). MGR is a member of the CONICET (Argentina).

References

1. Wormwell F, Booth GH (1964) Anti-Corros Method M 11:26–27
2. Videla HA (2000) Biofouling 15:37–47
3. Muthukumar N, Rajasekar A, Ponmariappan S, Mohanan S, Maruthamuthu S, Muralidharan S, Subramanian P, Palaniswamy N, Raghavan M (2003) Indian J Exp Biol 41:1012–1022
4. Zhao X, Duan J, Hou B, Wu S (2007) J Mater Sci Technol 23:323–328
5. Hamilton WA, Lee WB (1995) In: LL B (ed). Plenum Press, New York, pp 243–264
6. Hamilton WA (1985) Annu Rev Microbiol 39:195–217
7. Booth GH (1964) J Appl Bacteriol 27:174–181
8. King RA, Miller JD (1971) Nature 233:491–492
9. Cheung CWS, Beech IB (1996) Biofouling 9:231–249
10. Cheung CWS, Beech IB, Campbell SA, Satherley J, Schiffrin DJ (1994) Int Biodeter Biodegr 33:299–310
11. Lee M-H, Caffrey S, Voordouw J, Voordouw G (2010) Appl Microbiol Biotechnol 87:1109–1118
12. Shepherd JA, Waigh RD, Gilbert P (1988) Antimicrob Agents Chemother 32:1693–1698
13. Schaeufele P (1984) J Am Oil Chem Soc 61:387–389
14. Greene EA, Brunelle V, Jenneman GE, Voordouw G (2006) Appl Environ Microbiol 72:7897–7901
15. Nemati M, Mazutinec TJ, Jenneman GE, Voordouw G (2001) J Ind Microbiol Biotechnol 26:350–355
16. Nemati M, Jenneman GE, Voordouw G (2001) Biotechnol Prog 17:852–859
17. Biswas KC, Woodards NA, Xu H, Barton LL (2009) Biometals 22:131–139
18. Percival S (1999) J Ind Microbiol Biotechnol 23:112–117
19. Almendra MJ, Brondino CD, Gavel O, Pereira AS, Tavares P, Bursakov S, Duarte R, Caldeira J, Moura JJG, Moura I (1999) Biochemistry 38:16366–16372
20. Mota CS, Valette O, Gonzalez PJ, Brondino CD, Moura JJ, Moura I, Dolla A, Rivas MG (2011) J Bacteriol 193:2917–2923
21. Sebban C, Blanchard L, Bruschi M, Guerlesquin F (1995) FEMS Microbiol Lett 133:143–149
22. Costa C, Teixeira M, LeGall J, Moura JJG, Moura I (1997) J Biol Inorg Chem 2:198–208
23. González P, Rivas M, Brondino C, Bursakov S, Moura I, Moura JG (2006) J Biol Inorg Chem 11:609–616
24. Thapper A, Rivas MG, Brondino CD, Ollivier B, Fauque G, Moura I, Moura JJG (2006) J Inorg Biochem 100:44–50
25. Moura JJ, Xavier AV, Cammack R, Hall DO, Bruschi M, Le Gall J (1978) Biochem J 173:419–425
26. Andrade SLA, Brondino CD, Feio MJ, Moura I, Moura JJG (2000) Eur J Biochem 267:2054–2061

27. Rebelo J, Macieira S, Dias JM, Huber R, Ascenso CS, Rusnak F, Moura JJG, Moura I, Romão MJ (2000) J Mol Biol 297:135–146
28. Schwarz G, Mendel RR, Ribbe MW (2009) Nature 460:839–847
29. Mendel RR (2013) J Biol Chem 288:13165–13172
30. Grunden AM, Shanmugam KT (1997) Arch Microbiol 168:345–354
31. Grunden AM, Ray RM, Rosentel JK, Healy FG, Shanmugam KT (1996) J Bacteriol 178:735–744
32. Gonzalez PJ, Rivas MG, Mota CS, Brondino CD, Moura I, Moura JJG (2013) Coordin Chem Rev 257:315–331
33. Hauser LJ, Land ML, Brown SD, Larimer F, Keller KL, Rapp-Giles BJ, Price MN, Lin M, Bruce DC, Detter JC, Tapia R, Han CS, Goodwin LA, Cheng JF, Pitluck S, Copeland A, Lucas S, Nolan M, Lapidus AL, Palumbo AV, Wall JD (2011) J Bacteriol 193:4268–4269
34. Peck HD (1962) J Biol Chem 237:198–203
35. Postgate JR (1984) The sulfate-reducing bacteria. Cambridge University Press, London, pp 24–40
36. Heukeshoven J, Dernick R (1985) Electrophoresis 6:103–112
37. Dyballa N, Metzger S (2009) J Vis Exp 30:1431
38. Santos HM, Rial-Otero R, Fernandes L, Vale G, Rivas MG, Moura I, Capelo JL (2007) J Proteome Res 6:3393–3399
39. Zhang W, Culley DE, Scholten JC, Hogan M, Vitiritti L, Brockman FJ (2006) Anton Leeuw 89:221–237
40. Odom JM, Peck HD (1981) FEMS Microbiol Lett 12:47–50
41. Voordouw G (2002) J Bacteriol 184:5903–5911
42. Li X, Luo Q, Wofford NQ, Keller KL, McInerney MJ, Wall JD, Krumholz LR (2009) J Bacteriol 191:2675–2682
43. Venceslau SS, Lino RR, Pereira IA (2010) J Biol Chem 285:22774–22783
44. Pires RH, Lourenço AI, Morais F, Teixeira M, Xavier AV, Saraiva LGM, Pereira IAC (2003) BBA Bioenergetics 1605:67–82
45. Hedderich R, Hamann N, Bennati M (2005) Biol Chem 386:961–970
46. May HD, Patel PS, Ferry JG (1988) J Bacteriol 170:3384–3389
47. Pollock VV, Conover RC, Johnson MK, Barber MJ (2002) Arch Biochem Biophys 403:237–248
48. Sevcenco A-M, Bevers LE, Pinkse MWH, Krijger GC, Wolterbeek HT, Verhaert PDEM, Hagen WR, Hagedoorn P-L (2010) J Bacteriol 192:4143–4152
49. Gates AJ, Hughes RO, Sharp SR, Millington PD, Nilavongse A, Cole JA, Leach E-R, Jepson B, Richardson DJ, Butler CS (2003) FEMS Microbiol Lett 220:261–269
50. Hazen TC, Stahl DA (2006) Curr Opin Biotech 17:285–290
51. Zhou A, He Z, Redding-Johanson AM, Mukhopadhyay A, Hemme CL, Joachimiak MP, Luo F, Deng Y, Bender KS, He Q, Keasling JD, Stahl DA, Fields MW, Hazen TC, Arkin AP, Wall JD, Zhou J (2010) Environ Microbiol 12:2645–2657
52. Chhabra SR, He Q, Huang KH, Gaucher SP, Alm EJ, He Z, Hadi MZ, Hazen TC, Wall JD, Zhou J, Arkin AP, Singh AK (2006) J Bacteriol 188:1817–1828
53. He Q, He Z, Joyner DC, Joachimiak M, Price MN, Yang ZK, Yen HC, Hemme CL, Chen W, Fields MM, Stahl DA, Keasling JD, Keller M, Arkin AP, Hazen TC, Wall JD, Zhou J (2010) ISME J 4:1386–1397
54. Mukhopadhyay A, Redding AM, Joachimiak MP, Arkin AP, Borglin SE, Dehal PS, Chakraborty R, Geller JT, Hazen TC, He Q, Joyner DC, Martin VJJ, Wall JD, Yang ZK, Zhou J, Keasling JD (2007) J Bacteriol 189:5996–6010
55. Kazakov AE, Rajeev L, Luning EG, Zane GM, Siddartha K, Rodionov DA, Dubchak I, Arkin AP, Wall JD, Mukhopadhyay A, Novichkov PS (2013) J Bacteriol 195:4466–4475
56. Fournier M, Aubert C, Dermoun Z, Durand MC, Moinier D, Dolla A (2006) Biochimie 88:85–94
57. Marston AL, Errington J (1999) Mol Microbiol 33:84–96
58. Hayashi I, Oyama T, Morikawa K (2001) EMBO J 20:1819–1828
59. Morita Y, Sobel ML, Poole K (2006) J Bacteriol 188:1847–1855
60. Tomei F, Barton L, Lemanski C, Zocco T, Fink N, Sillerud L (1995) J Ind Microbiol 14:329–336
61. Hayat J (1989) Principles and techniques of electron microscopy: biological applications. Macmillan Press, London
62. Chen B-Y, Utgikar VP, Harmon SM, Tabak HH, Bishop DF, Govind R (2000) Int Biodeter Biodegr 46:11–18
63. Chamberlain AHL (1992) In: Melo LF, Bott TR, Fletcher M, Capdeville B (eds) Biofilms—science and technology. Springer, Netherlands, pp 59–67